Check for updates

Journal of Applied Polymer Science

WILEY

Applied Polymer SCIENCE

RESEARCH ARTICLE

Enhanced Multifunctional Properties of Polypropylene/Bi_2O_3 Nanocomposites for Energy Storage and Packaging Applications

Emre Beyazay[1] | Nazlıcan Şahin Sütcü[2] | Ayşe Nur Şahin[1] | Yaşar Karabul[1] | Mehmet Kılıç[1] | Zeynep Güven Özdemir[1]

[1]Department of Physics, Yildiz Technical University, Istanbul, Turkey | [2]Department of Physics, Marmara University, Istanbul, Turkey

Correspondence: Zeynep Güven Özdemir (zgozdemir@gmail.com; zguven@yildiz.edu.tr)

Received: 11 August 2025 | **Revised:** 19 October 2025 | **Accepted:** 28 October 2025

Funding: This work was supported by the Yildiz Technical University Scientific Research Projects Coordination Department (FBA-2020-4003).

Keywords: dielectric properties | mechanical properties | optical properties

ABSTRACT

This study reports the development of multifunctional polypropylene (PP) nanocomposites reinforced with Bi_2O_3 nanoparticles synthesized via the solvothermal method. Structural characterization of Bi_2O_3 was carried out by XRD, TEM, and FTIR. Nanocomposites containing 0.5–5 wt% Bi_2O_3 were fabricated using extrusion and hot-pressing, and their optical, morphological, electrical, and mechanical properties were systematically investigated. UV–Vis analyses revealed a reduction in band gap and an increase in refractive index, extinction coefficient, and optical conductivity with increasing Bi_2O_3 content. Electrical measurements indicated improved energy storage capability, particularly at 5 wt% Bi_2O_3 loading, while maintaining low dielectric loss. Mechanical tensile tests showed that 5 wt% Bi_2O_3 increased Young's modulus by 49.5% compared to pure PP, improving stiffness and rigidity, whereas 0.5 wt% Bi_2O_3 enhanced stress at break and strain at break, indicating improved toughness and ductility. Wettability measurements revealed a hydrophobic transition at 0.5 wt% and a return to hydrophilic behavior at higher loadings, consistent with surface roughness trends. Overall, the results demonstrate that Bi_2O_3 nanoparticle-reinforced PP nanocomposites exhibit synergistic improvements in optical, dielectric, and mechanical performance, making them promising candidates for lightweight structural components, durable flexible packaging, and advanced dielectric energy storage devices.

1 | Introduction

In the industrial sense, it is critical to develop materials that are always lighter, more robust in terms of mechanical properties, adjustable electrical properties, and low cost that can be used for multiple purposes. For this purpose, polymers whose mechanical and electrical properties were modified with various filling and reinforcing materials were preferred for a long time. As it is known, the effect of the reinforcing material addition to the polymer is inversely proportional to the size of the filling material and changes in direct proportion to its ratio in the polymer matrix. In particular, materials with better mechanical and electrical properties can be obtained by adding nanoparticles to thermoplastic polymers at low concentrations compared to conventional composites [1–6]. Therefore, the development of thermoplastic nanocomposites, which blend the lightness and flexibility of polymers with the superior electrical and mechanical properties of nano-sized fillers, provides important contributions to both polymer nanotechnology and a wide range of applications from medicine to the automotive sector. Numerous studies have reported significant advances in the design of polymer nanocomposites with enhanced mechanical and functional properties. For instance, acrylonitrile butadiene styrene (ABS) reinforced with multiwalled carbon nanotubes (MWCNTs) has been successfully fabricated via fused deposition modeling (FDM). These ABS/MWCNT nanocomposites demonstrated

© 2025 Wiley Periodicals LLC.

remarkable improvements in tensile strength and modulus due to the uniform dispersion of nanotubes, though at the expense of ductility [7]. This highlights the role of nano-filler dispersion and interfacial bonding in dictating the trade-off between strength and flexibility in thermoplastic-based nanocomposites. Such examples from polymer systems can be compared with metallic hybrid composites, where reinforcement strategies are similarly used to tailor multifunctional performance.

Similarly, aluminum alloy (Al7029)-based hybrid composites reinforced with tungsten carbide and fly ash have been synthesized through liquid metallurgy. The incorporation of dual reinforcements led to simultaneous increases in hardness and tensile strength, while microstructural observations confirmed a transition from ductile to brittle fracture behavior with higher reinforcement loadings [8]. These results further confirm the versatility of nanoparticle incorporation strategies in tailoring multifunctional properties of both polymers and metals. While metallic systems illustrate the mechanical enhancement potential, polymer-based nanocomposites also continue to evolve toward multifunctionality, not only in mechanics but also in optics. In addition to the widely studied metal oxide and ceramic nanoparticles, recent work has also focused on the development of luminescent halide-based polymer nanocomposites for optoelectronic applications. For example, Cs_4PbBr_6/poly(vinylidene difluoride) (PVDF) nanocomposites have been reported to exhibit a unique combination of green luminescence, hydrophobicity, and mechanical flexibility, making them suitable for photonic and display technologies. The incorporation of 0-D cesium lead bromide nanoparticles into a PVDF matrix resulted in improved optical emission efficiency along with robust environmental stability, highlighting the potential of multifunctional polymer–inorganic hybrid systems to address challenges in advanced optoelectronic devices [9]. These optical case studies further underline the versatility of polymer nanocomposites and motivate the exploration of new fillers in conventional matrices such as polypropylene. Therefore, after reviewing both mechanical and optical approaches in different systems, it becomes evident that polypropylene-based nanocomposites still hold unique importance as cost-effective, lightweight, and widely used materials.

In particular, as the need for easy-to-process, stronger, lighter, versatile, and cheaper materials for industrial applications increases, PP nanocomposites will continue to offer significant advantages to meet these requirements. In this context, it is aimed to strengthen the electrical and mechanical properties of PP, which is one of the most used thermoplastic polymers industrially, with a nanoparticle to be synthesized.

When the scientific literature is investigated in terms of PP-based nanocomposites prepared to improve the electrical and mechanical properties of PP, nano-clay [10], nano-clay functionalized with Fe nanoparticles [11], nano-Al_2O_3 particles [12], graphene oxide functionalized with SiO_2 [13], nano-calcium carbonate particles [14, 15], nano-calcium carbonate and glass fiber 1–6 [16], nano-TiO_2 [17], carbon nanotubes (CNTs) [18], CNTs decorated with C60 [19], the combined usage of MWCNTs and barium titanate [20], rattan nanofibers [21], and nano-cellulose [22] are among the frequently used reinforcements that draw attention. For example, when the mechanical properties of PP reinforced with Al_2O_3 nanoparticle additives were examined, it was determined that the tensile strength (tensile strength) increased by 1% in the case of 3%–5% by mass Al_2O_3 nanoparticle additives. On the other hand, it was reported that the elongation at break value decreases by 50% in the same additive states [12]. In another scientific study investigating how the thermal and mechanical properties of PP change with graphene oxide functionalized with nano-SiO_2 particles, it was stated that the related reinforcement increased the tensile strength value of PP by approximately 27% and its thermal properties were also improved [13]. In the article in which the effect of nano-clay reinforcement containing Fe nanoparticles on the mechanical properties of PP was examined by Khalaj et al., it was reported that remarkable improvements were observed in the tensile strength and elongation properties of PP, but an increase in yield strength and brittleness was detected [11]. In addition, recent studies have emphasized dielectric performance improvements in PP-based nanocomposites. For instance, polypropylene-graft-maleic anhydride/organic Na^+−montmorillonite films showed enhanced permittivity with a discharged energy density of 5.2 J cm^{-3}, underlining their potential for high-energy-density capacitors [23]. Recently, highly dispersed graphene nanoplatelets in PP were shown to significantly improve dielectric properties while providing frequency-selective electromagnetic interference shielding, broadening the application spectrum of PP nanocomposites [24]. On the other hand, it was determined by Eiras and Pessan that a 3% nano-calcium carbonate particle additive caused a 0.5% and 1.5% increase in elastic modulus and yield stress values of PP, respectively [18]. Aydemir et al. also reported that the degree of crystallinity, which has a significant effect on the mechanical properties, increases for PP with the addition of nano-TiO_2 [17]. In another study investigating the effect of nanocellular fibril (NSF) reinforcement on the mechanical properties of PP, it was determined that the Young's modulus of PP/NSF composite with 0.1% mass chemical compatibilizer added increased by 87% compared to pure PP [22]. However, the effect of nanoparticle additives used in these articles, whose important results were expressed above, on the dielectric properties of PP has not been investigated. On the other hand, in a research paper focused on the dielectric properties of PP/MWCNT composites, it was reported that the dielectric constant of PP/5% MWCNT nanocomposite is greater than 110 in the low-frequency region and has a low dielectric loss. Additionally, Tserpes et al. showed that 2%–5% MWCNT filler increased both Young's modulus and yield strain values of PP by more than 20% [25]. Also, Yu et al. have reported that PP/MWCNT/Barium titanate triple nanocomposite containing 57% PP, 40% Barium titanate, and 3% MWCNT becomes electrically conductive. However, the effect of the related nano-additives on the mechanical properties of PP has not been investigated [20]. In addition to these studies, Azmi et al. studied the influence of $MgAl_2O_4$, $CaCO_3$, and surface-modified $CaCO_3$ nanofillers on both the structure and dielectric properties of PP. They showed that PP/surface-modified $CaCO_3$ nanocomposite has the highest breakdown strength among others [26]. Very recently, Lee et al., achieved the preparation of PP/graphene nanoplatelet composites with high dispersion of nanoplatelets and studied the dielectric properties of the composites. They showed that as the graphene nanoplatelets' agglomeration size reduces, considerable improvement can be possible in dielectric loss [27]. As can be seen, current studies were carried out in the scientific literature on improving the mechanical and electrical properties of PP and many different nanoparticles are used as reinforcements. However, the electrical and mechanical properties of PP

10974628, 0, Downloaded from https://onlinelibrary.wiley.com/doi/10.1002/app.58192 by Zeynep Guven Ozdemir - Yildiz Teknik University , Wiley Online Library on [08/11/2025]. See the Terms and Conditions (https://onlinelibrary.wiley.com/terms-and-conditions) on Wiley Online Library for rules of use; OA articles are governed by the applicable Creative Commons License

still need to be improved. For this purpose, Bi_2O_3 nanoparticles (n-Bi_2O_3) with high mechanical strength and nontoxicity, which have not been tested for PP in the literature until now, were used in this study. Another reason for choosing Bi_2O_3 as a nanoparticle additive is its high charge carrier mobility along with thermal and mechanical stabilities. In this context, the incorporation of Bi_2O_3 nanoparticles, which is a metal oxide semiconductor, into a polymer will cause significant changes in the structural, electrical, mechanical, and optical properties of the polymer as a result of polymer–inorganic nanoparticle interface interactions.

2 | Experimental Details

2.1 | Materials

PP granules, the main component of composites, are of technical quality and were obtained from Petkim Industry. The molecular weight of the PP granules used is 42.08 g/mol, the melting temperature is 165°C and the bulk density is 0.905 g/cm^3. Bi_2O_3 nanoparticles, which were used to reinforce the PP polymer, were synthesized by the solvothermal method. Bismuth nitrate pentahydrate with a purity of 98% (CAS:10035-06-0) and ethylene glycol (RPE—for analysis CAS:107-21-1), which were the precursor materials in the Bi_2O_3 nanoparticle synthesis, were supplied by Sigma-Aldrich (Darmstadt, Germany) and Carlo Elba (Emmendingen, Germany) companies, respectively.

2.2 | Methods

The crystallographic structure and the lattice parameters of the Bi_2O_3 nanoparticles were determined by the Rigaku model x-ray diffraction (XRD) device that produces x-rays with a wavelength of 1.5406×10^{-10} (m). The size of Bi_2O_3 nanoparticles was identified with transmission electron microscopy (TEM) analysis by using the JEOL JEM 1220 TEM device. The surface roughness of the films was determined by examining the 3D surface images of the samples obtained by the atomic force microscope (AFM) Workshop TT model AFM. The morphology of the pure PP and the nanocomposites was viewed by Thermo Scientific Apreo 2S scanning electron microscope (SEM). The wettability behavior of the composite surfaces was characterized by static contact angle (CA) measurements using an Attension Theta Lite optical tensiometer equipped with a high-resolution camera, and the average CA values were determined from three different points on each sample. The FTIR spectra of the components of the composites and composites were analyzed by Bruker TENSOR 27 FTIR spectrometer within the 600–4000 cm^{-1} wavenumber. The UV–Vis light absorption spectra of the pure PP and the composites were measured by Perkin Elmer Lambda 35 UV/Vis spectrometer within the wavelength range of 200–1100 nm at room temperature. Frequency-dependent electrical properties of the composites were measured with a Wayne Kerr brand 6500B model impedance analyzer in the frequency range of 20 Hz to 15 MHz. Measurements were made at room temperature by using circular-shaped gold electrodes with a diameter of 7.236 mm. A parallel plate capacitor structure was formed by placing the composite thick films produced between the gold electrodes, and an electric field with a frequency varying from 50 Hz to 0.1 MHz was applied to this structure. The mechanical tensile tests of the produced film samples have also been carried out with a computer-connected LABOMAK brand mechanical strength device at room temperature.

2.3 | Synthesis of Bi_2O_3 Nanoparticles and Their Structural Properties

Ethylene glycol was used as a solvent for bismuth nitrate pentahydrate for the synthesis of Bi_2O_3 nanoparticles by the solvothermal method. After 0.73 g of bismuth nitrate pentahydrate was dissolved in 50 mL of ethylene glycol, stirring was carried out at 1000 rpm in a magnetic stirrer for 1 h. Then, the solution was placed in the autoclave, and the autoclave was kept in the oven at 200°C for 12 h. After this process, a dark precipitate was obtained. This precipitate was washed first with distilled water and then with ethanol. The Bi_2O_3 powder obtained after the cleaning process was dried in an oven at 80°C. Finally, the synthesis was completed by an annealing process at 500°C for 4 h.

Following the synthesis step, XRD analysis was performed to confirm that the obtained particles were Bi_2O_3; TEM images have also been examined for particle size determination. In addition, FTIR spectra of the Bi_2O_3 were analyzed when the composites' FTIR spectra were investigated.

The XRD pattern of the Bi_2O_3 nanoparticles synthesized is given between $2\theta = 20°–70°$ in Figure 1. The XRD analysis performed by X'Pert HighScore Plus software revealed that the particles crystallize in a monoclinic structure with the P1 21/c 1 space group and the lattice parameters of $a = 5.8490$ Å, $b = 8.1660$ Å, $c = 7.5100$ Å. Additionally, the XRD pattern is in good agreement with the Bi_2O_3 structure.

Figure 2 displays the TEM image of the synthesized Bi_2O_3 nanoparticles. The particles exhibited deformed spherical morphology with an average diameter in the range of ~20–40 nm. The micrograph confirms the relatively narrow size distribution, which is crucial for achieving uniform physical and dielectric properties when incorporated into polymer matrices.

2.4 | Preparation of the Composites

Several different techniques were tried during the production of PP-based, thick-film reinforced composite with Bi_2O_3

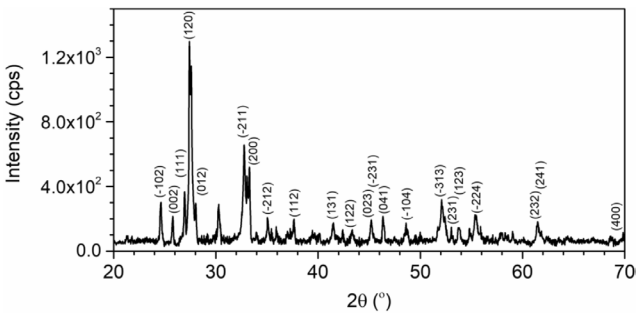


FIGURE 1 | The XRD pattern of the Bi_2O_3 nanoparticles between $2\theta = 20°–70°$. [Color figure can be viewed at wileyonlinelibrary.com]

10974628, 0, Downloaded from https://onlinelibrary.wiley.com/doi/10.1002/app.58192 by Zeynep Guven Ozdemir - Yildiz Teknik University , Wiley Online Library on [08/11/2025]. See the Terms and Conditions (https://onlinelibrary.wiley.com/terms-and-conditions) on Wiley Online Library for rules of use; OA articles are governed by the applicable Creative Commons License

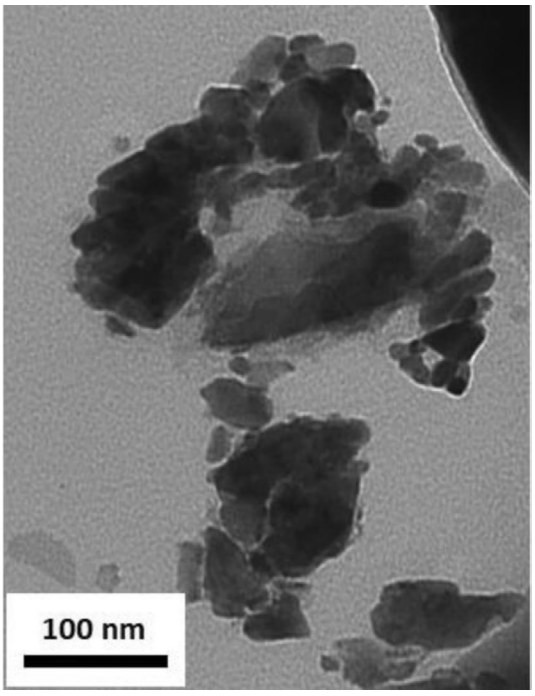


FIGURE 2 | The TEM image of the Bi_2O_3 nanoparticles.

nanoparticles, and the most homogeneous nanoparticle distribution and the most homogeneous thickness were obtained by using a single screw extruder.

First, PP in the form of granules was pulverized with a grinder. To prepare PP-based composites, different weight percentages (0.5%, 1%, 3%, and 5%) of Bi_2O_3 nanoparticle reinforcement powder were added to the PP powder, and the mixtures were processed in a single screw extruder. The process in the single screw extruder was repeated two times to obtain homogeneous mixtures. Then, the samples were placed in a circular Teflon mold and hot pressed between 165°C and 175°C. The diameter of the mold used was 7 cm and the thickness of the samples varied between 8 μm and 12 μm. Also, for reference, the same procedure outlined above was followed when preparing a pure PP sample in thick film form.

The surface topology of the samples has been examined by AFM images given in Figure 3. The AFM images were obtained by scanning the 10 μm × 10 μm surface area of each film. As shown in Figure 3, the surface of the pure PP film has some peak clusters. On the other hand, the composites' surfaces have fewer peak clusters with decreased heights compared with the pure PP. Additionally, this tendency becomes more apparent when the root mean square roughness (S_q) values are examined.

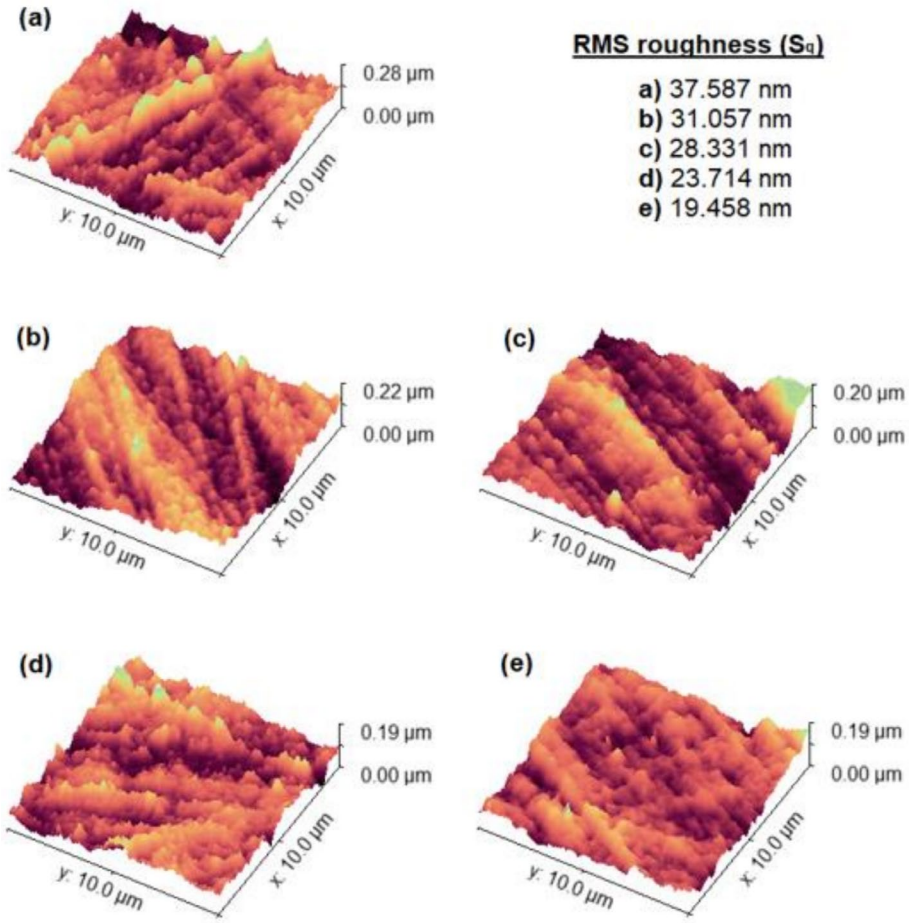


FIGURE 3 | The AFM images of the (a) pure PP, (b) PP/0.5% n-Bi_2O_3, (c) PP/1% n-Bi_2O_3, (d) PP/3% n-Bi_2O_3, and (e) PP/5% n-Bi_2O_3. [Color figure can be viewed at wileyonlinelibrary.com]

10974628, 0, Downloaded from https://onlinelibrary.wiley.com/doi/10.1002/app.58192 by Zeynep Guven Ozdemir - Yildiz Teknik University , Wiley Online Library on [08/11/2025]. See the Terms and Conditions (https://onlinelibrary.wiley.com/terms-and-conditions) on Wiley Online Library for rules of use; OA articles are governed by the applicable Creative Commons License

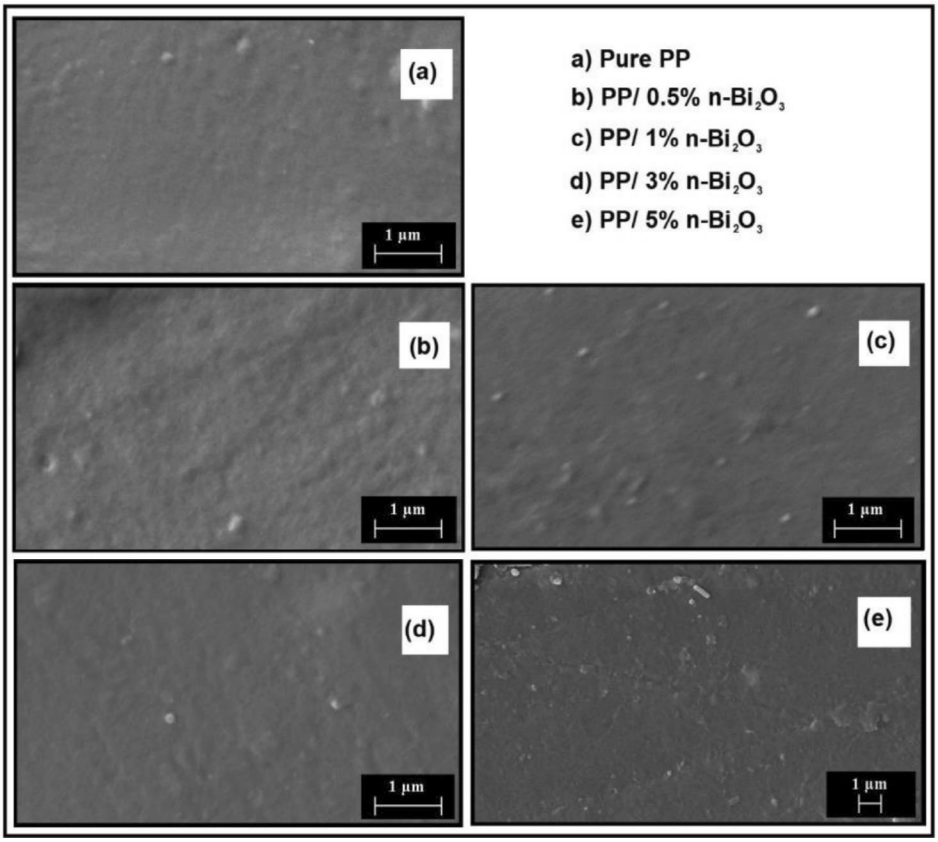


FIGURE 4 | SEM micrographs of (a) neat PP, (b) PP/0.5 wt% Bi_2O_3, (c) PP/1 wt% Bi_2O_3, (d) PP/3 wt% Bi_2O_3, and (e) PP/5 wt% Bi_2O_3 nanocomposites.

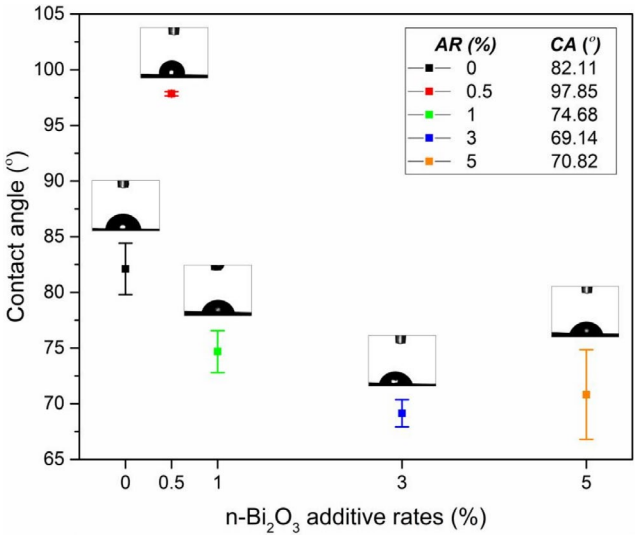


FIGURE 5 | Water contact angle of neat PP film and PP/BaO nanocomposite films. [Color figure can be viewed at wileyonlinelibrary.com]

As shown in Figure 3, the S_q value of the pure PP is 31.587 nm. However, the gradual increase in Bi_2O_3 nanoparticle contribution in the PP leads to hierarchical decreases in S_q values. The lowest S_q value has been recorded as 19.458 nm for the 5% n-Bi_2O_3 additive case. The smoother surface in the composites implies that some of the gaps and/or irregularities on the surface may be filled with Bi_2O_3 nanoparticles.

2.5 | Morphological Analysis

SEM micrographs (Figure 4) reveal that the neat PP exhibits a smooth and featureless surface, which is typical of thermoplastic polymers. Upon incorporating Bi_2O_3 nanoparticles, the nanoparticles are distinguishable. At low loadings (0.5–1 wt%), the nanoparticles are homogeneously dispersed without noticeable agglomeration, indicating good interfacial compatibility. Increasing the nanoparticle content to 5 wt% leads to partial agglomeration and localized surface irregularities, which are consistent with filler crowding at higher concentrations.

2.6 | Wettability Behavior of the Samples

The wettability of the neat PP and PP/Bi_2O_3 nanocomposites was evaluated through static CA measurements at 22°C using the sessile drop method with a droplet volume of approximately 5 µL. As illustrated in Figure 5, the pure PP exhibited a CA of 82.1°, indicating low wettability but still within the hydrophilic range ($\theta < 90°$) [28]. At 0.5 wt% Bi_2O_3, the CA increased significantly to 97.8°, indicating a transition from hydrophilic to hydrophobic behavior, consistent with Cassie–Baxter wetting, where micro/nano-texturing traps air and reduces the solid–liquid fraction, thereby increasing the apparent CA [29–31]. However, when the filler content was increased to 1, 3, and 5 wt%, the CA decreased to 74.7°, 69.1°, and 70.8°, respectively, indicating a reverse transition toward hydrophilic wetting, which correlates well with the reduction in S_q values and a shift toward Wenzel-type wetting.

10974628, 0, Downloaded from https://onlinelibrary.wiley.com/doi/10.1002/app.58192 by Zeynep Guven Ozdemir - Yildiz Teknik University , Wiley Online Library on [08/11/2025]. See the Terms and Conditions (https://onlinelibrary.wiley.com/terms-and-conditions) on Wiley Online Library for rules of use; OA articles are governed by the applicable Creative Commons License

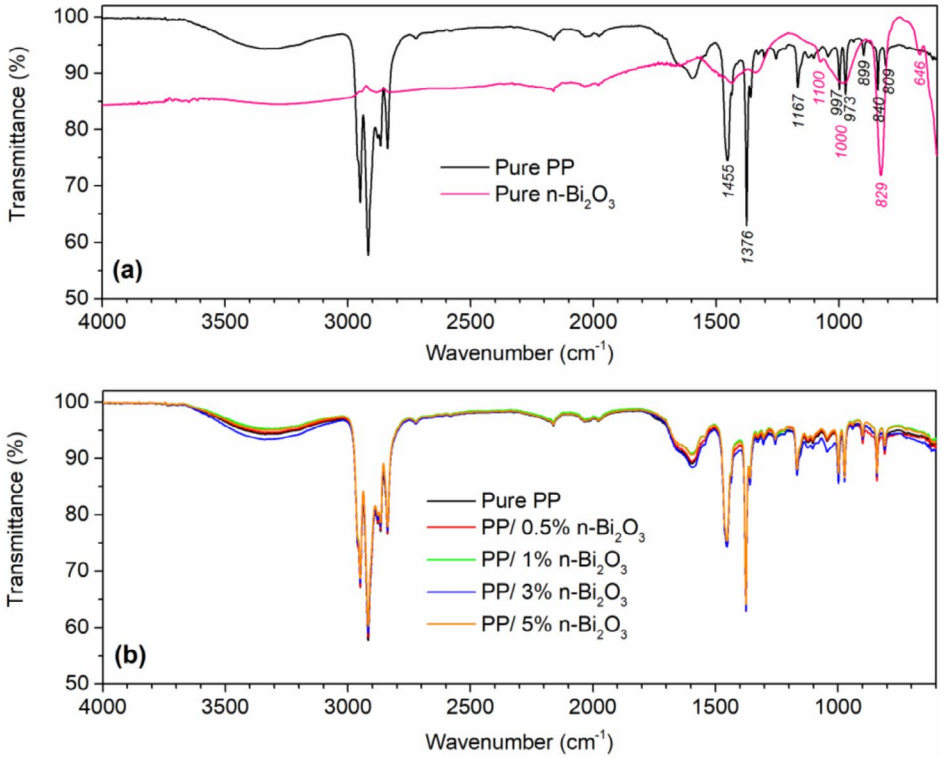


FIGURE 6 | The FTIR spectra of (a) the pure PP and pure nano-Bi_2O_3 particles and (b) the composites. [Color figure can be viewed at wileyonlinelibrary.com]

This trend is strongly supported by the surface roughness results obtained from AFM analysis. The root mean square roughness of neat PP was 31.6 nm, decreasing steadily with increasing Bi_2O_3 content to 19.5 nm at 5 wt%. This reduction reflects a progressive smoothing of the surface as nanoparticles fill microvoids and irregularities, leading to a more homogeneous topography. As the surface becomes smoother, the wetting behavior shifts from Cassie–Baxter to Wenzel wetting, where the roughness amplifies the intrinsic surface chemistry and facilitates liquid spreading on higher-energy domains [32, 33]. The slight increase in CA observed at 5 wt% is likely associated with local nanoparticle agglomeration, which reintroduces limited heterogeneity despite the overall smoother surface. Altogether, these findings reveal a clear relationship between nanoparticle loading, surface topography, and wettability, demonstrating that wetting behavior can be effectively tuned by controlling Bi_2O_3 content and surface morphology.

3 | Results

3.1 | FTIR Analysis

To analyze the addition of Bi_2O_3 nanoparticles to the PP matrix, Figure 6a primarily considers the pure PP and pure Bi_2O_3 nanoparticles' FTIR spectra. As can be seen from Figure 4a, characteristic bands between 3000 and 2800 cm^{-1} correspond to asymmetrical C–H stretching vibrations and symmetrical C–H stretching vibrations in CH_3, CH_2, and CH groups [34]. The bands at 1455 and 1376 cm^{-1} correspond to the CH_2 symmetric bending and CH_3 symmetric bending, respectively [35]. The band observed at 1167 cm^{-1} is consistent with C–C chain tension, C–H swinging, and CH_3 swing vibrations. However, bands at 997, 973, and 899 cm^{-1} indicate CH_3 swinging and the presence of C–C chain stretching vibrations. The band at 840 cm^{-1} is attributed to CH_2 oscillation and C–CH_3 stretching vibrations. The last prominent band detected at 809 cm^{-1} corresponds to C–C stretching and CH_2 swinging modes [36, 37]. Thus, the FTIR spectrum obtained for the PP sample was found to be compatible with the scientific literature.

When the FTIR spectrum of the nano-Bi_2O_3 particles given in Figure 6a is evaluated, the broad and low-intensity band between 3500 and 3000 cm^{-1} is a characteristic stretching vibration of the O–H group. The transmittance band that appeared in the vicinity of 1100 cm^{-1} can also be attributed to the normal OH stretching vibration of H_2O in the Bi–O lattice [38]. Besides, if it is remembered that the characteristic FTIR bands for Bi_2O_3 metal oxide are below 1000 cm^{-1}, the two bands observed around 829 and 646 cm^{-1} indicate the stretching and bending vibrations of the bismuth-oxygen bond, respectively [39].

According to Figure 6b, the FTIR spectra of PP/Bi_2O_3 nanocomposites exhibit characteristic bands of PP but also have weaker bands of Bi_2O_3 due to increased Bi_2O_3 nanoparticle contribution. For example, shifts observed in the characteristic bands of PP around 829 and 646 cm^{-1} indicate the stretching and bending vibrations of the bismuth–oxygen bond, respectively, in the nanocomposites. These shifts suggest an existing interaction between PP and Bi_2O_3 particles.

3.2 | Analysis of Optical Properties

The optical properties of the samples were evaluated in the context of UV–Vis light absorption, transmittance, and reflectance spectra. The UV–Vis light absorption spectra of the pure PP and

10974628, 0, Downloaded from https://onlinelibrary.wiley.com/doi/10.1002/app.58192 by Zeynep Guven Ozdemir - Yildiz Teknik University , Wiley Online Library on [08/11/2025]. See the Terms and Conditions (https://onlinelibrary.wiley.com/terms-and-conditions) on Wiley Online Library for rules of use; OA articles are governed by the applicable Creative Commons License

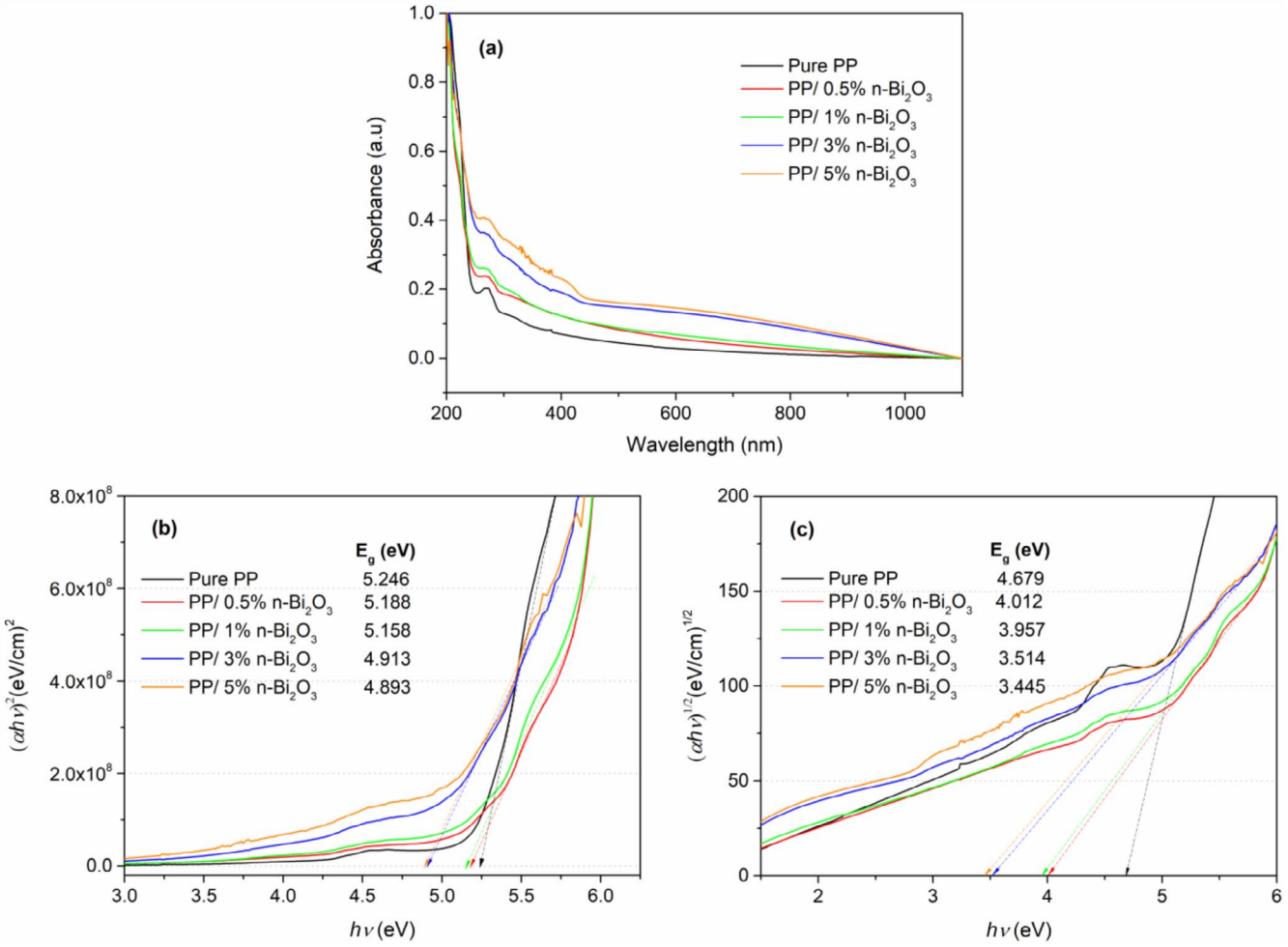


FIGURE 7 | (a) The UV–Vis light absorption spectra, (b) $(\alpha h\nu)^2$ versus $h\nu$, and (c) $(\alpha h\nu)^{1/2}$ versus $h\nu$ plots of the samples. [Color figure can be viewed at wileyonlinelibrary.com]

the PP-based Bi_2O_3 reinforced nanocomposites are shown in Figure 7a. As illustrated in Figure 7a, the absorption intensity of the absorption curves increases hierarchically with the increasing Bi_2O_3 nanoparticle additive percentage. This behavior can be interpreted as the increase in the number of charge carriers in composites relative to pure PP. Additionally, the absorption edge gradually shifts toward the higher wavelength as the nanoparticle contribution increases. A similar behavior was reported for SnO_2 nanoparticles doped high-density polyethylene nanocomposites by Anu and Pillai [40]. Additionally, the UV–Vis light absorption spectra of the PP/Bi_2O_3 nanocomposites that exhibited higher absorption intensity values in the visible region compared with the pure PP and an observable change in their color, indicate the modified UV–Vis light absorption properties of PP due to the addition.

To estimate the direct and indirect transition energy band gap of the pure PP and the composites, the Tauc's plots (i.e., the versus energy curves) of the samples were drawn and shown in Figure 7b,c, respectively. As shown in Figure 7b, the absorption edge of the PP shifted toward the lower photon energy as the nanoparticle additive concentration increased from 0% to 5%. The direct and indirect optical band gap (E_g) were calculated by using Equations (1) and (2), respectively.

$$(\alpha h\nu)^2 = A\left[h\nu - E_g\right] \tag{1}$$

$$(\alpha h\nu)^{1/2} = A\left[h\nu - E_g\right] \tag{2}$$

where α is the absorption coefficient, $h\nu$ represents the incident photon energy, and A is the proportionality constant. The band gap values of the samples were estimated by the extrapolation of the linear region of the Tauc's plots onto the x-axis. The direct band gap of the pure PP was determined as 5.246 eV. Then, as is tabulated in Figure 7b, with the gradual increase in Bi_2O_3 nanoparticle additive, the band gap energy decreases hierarchically. As is known, when the size of nanoparticles approaches the nanoscale, quantum confinement effects become significant. Since smaller nanoparticles have a higher surface-to-volume ratio, leading to quantum confinement of charge carriers. This confinement can result in an increase in the effective mass of electrons and holes, causing a decrease in the band gap. Additionally, the interaction between the PP matrix and the Bi_2O_3 nanoparticles can affect the electronic structure of the PP, influencing the band gap. Interfacial interactions and charge transfer between the PP and the Bi_2O_3 nanoparticles can modify the energy levels. On the other hand, when Figure 7b,c are compared, it has been observed

10974628, 0, Downloaded from https://onlinelibrary.wiley.com/doi/10.1002/app.58192 by Zeynep Guven Ozdemir - Yildiz Teknik University , Wiley Online Library on [08/11/2025]. See the Terms and Conditions (https://onlinelibrary.wiley.com/terms-and-conditions) on Wiley Online Library for rules of use; OA articles are governed by the applicable Creative Commons License

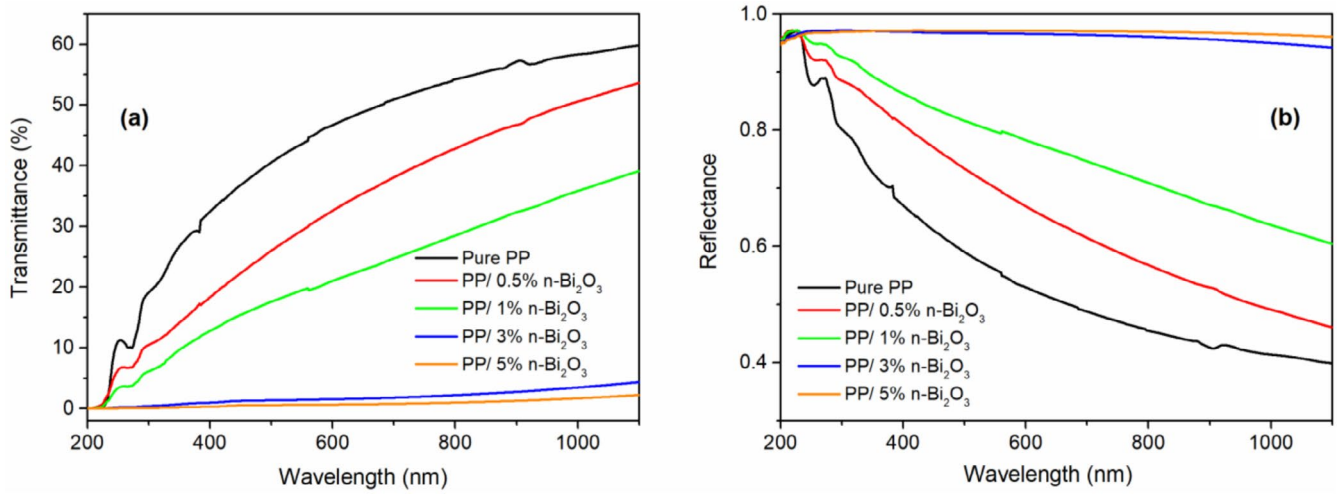


FIGURE 8 | (a) The UV–Vis light transmittance and (b) reflectance spectra of the samples. [Color figure can be viewed at wileyonlinelibrary.com]

that the plots are linear over a wide range of photon energy in Figure 7b, which was used to calculate the direct band gap energy. Additionally, considering the zero intersection of the curve, it can be concluded that the composites exhibit a direct type of transition [9].

As a second optical analysis, the refractive index (n) and extinction coefficient (k), which are considered as the "fingerprint" of a material, were calculated for the samples. As is known, n and k are related to the interaction between the material and incoming light. While n is related to refraction, k is calculated by using the absorption process. To calculate these parameters, the transmittance Eand reflectance spectra of the samples were shown in Figures 8a and 8b, respectively.

As shown in Figure 8a, the transmittance of the PP exhibits a gradual decreasing trend with increasing Bi_2O_3 nanoparticle additive. The decrease in transmittance is a result of the nanoparticles scattering and absorbing light as the light passes through the material. As the nanoparticles are introduced, they scatter light in various directions, preventing some of it from passing through the material. This scattering effect can reduce the transmittance. On the other hand, as illustrated in Figure 8b, the reflectance of the pure PP increases hierarchically due to nanoparticle additives. The increase in reflectance, coupled with a decrease in transmittance due to the contribution of nanoparticles for the PP matrix, indicates that the nanoparticles in the material are scattering incident light, causing some of it to be redirected back, rather than allowing it to pass through.

The refractive index (n) values for the pure PP and PP-based Bi_2O_3 reinforced nanocomposites at different wavelengths were calculated by using the reflection coefficient, R:

$$n = \left[1 + (R)^{1/2}\right]\left[1 - (R)^{1/2}\right]^{-1} \quad (3)$$

The extinction coefficient, k has also been calculated by Equation (4).

$$k = \alpha\lambda(4\pi)^{-1} \quad (4)$$

where α is the absorption coefficient at λ wavelength. The variations of the refractive indexes and the extinction coefficients of the samples with wavelength were given in Figure 9a and 9b, respectively.

As shown in Figure 9a, the refractive indices of the pure PP, and the composites having 0.5% and 1% Bi_2O_3 nanoparticle contribution first increase and then decrease considerably with the increase of wavelength of the incident light. On the other hand, the same characteristic was observed in the refractive index for the 3% and 5% Bi_2O_3 added composites; however, with increasing wavelength, a sharp decrease was replaced by a slight decrease. This behavior indicates that there is no anomalous refractivity for the visible light range for the samples [41]. Moreover, the refractive index of the PP matrix increases gradually as the Bi_2O_3 nanoparticle contribution increases. The increase in refractive index is an indication that the composite material has become more optically dense. As it is known, the refractive index is a measure of how much light bends or slows down as it passes through a material. An increase in the refractive index indicates that the light bends more. Additionally, the higher refractive index observed in composites can also be interpreted as better confinement of light within the composite material. As shown in Figure 9b, the increase in the refractive index in the wavelength range studied is accompanied by an increase in the k coefficient. The increase in the extinction coefficient implies that more light is being absorbed by the material due to the Bi_2O_3 nanoparticle additive. This combination leads to a higher optical density for the composites, meaning that the material has a stronger interaction with light. The fact that such a feature is obtained by adding Bi_2O_3 nanoparticles may be valuable for applications where light absorption is desired, such as photo detectors.

Using the data on the wavelength changes of n and k, the real (ε_1) and imaginary parts (ε_2) of the dielectric constant have also been calculated for the same wavelength range by Equations (5) and (6):

$$\varepsilon_1 = n^2 - k^2 \quad (5)$$

$$\varepsilon_2 = 2nk \quad (6)$$

10974628, 0, Downloaded from https://onlinelibrary.wiley.com/doi/10.1002/app.58192 by Zeynep Guven Ozdemir - Yildiz Teknik University , Wiley Online Library on [08/11/2025]. See the Terms and Conditions (https://onlinelibrary.wiley.com/terms-and-conditions) on Wiley Online Library for rules of use; OA articles are governed by the applicable Creative Commons License

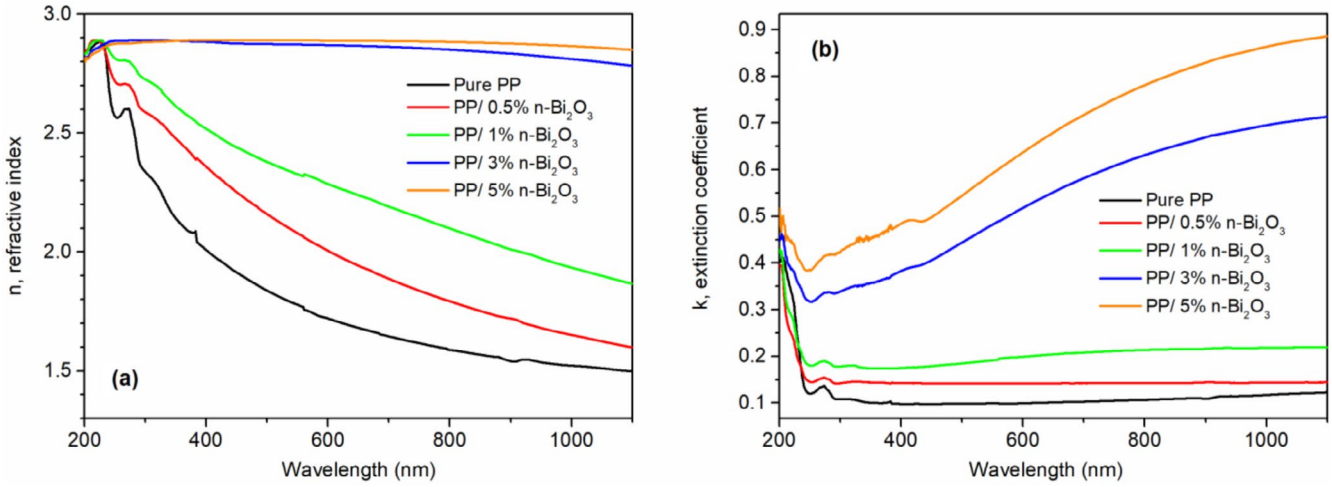


FIGURE 9 | The change of (a) the refractive index and (b) extinction coefficient with wavelength of the samples. [Color figure can be viewed at wileyonlinelibrary.com]

The variations of ε_1 and ε_2 with UV–Vis wavelength range were shown in Figure 10a and 10b, respectively.

As is illustrated in Figure 10a,b, the values of the real part of the dielectric constant are higher as compared to the imaginary part of the dielectric constant for all samples. Additionally, the ε_1 of the pure PP increases with increasing Bi_2O_3 nanoparticle contribution. This behavior implies that the electric flux density of PP film increases due to Bi_2O_3 nanoparticle additive [42]. Moreover, as can be noticed from Figure 10b, increasing ε_2 values were recorded because of the increasing nanoparticle contribution in accordance with the high k and n values for the composites according to Equation (5). Moreover, the electron energy loss (L) that is a quantity used in the study of interactions between electrons and matter, It describes the probability of an electron losing energy through inelastic scattering when passing through a material. L is defined by Equation (7)

$$L = \varepsilon_1\left[{\varepsilon_1}^2 + {\varepsilon_2}^2\right]^{-1} \tag{7}$$

The variations of electron energy loss with wavelength for the samples were shown in Figure 10c. It was determined that pure PP has the highest electron energy loss for all wavelengths studied among all samples. Additionally, the electron energy loss values of the composite films decrease hierarchically with the gradual increase of Bi_2O_3 nanoparticle addition.

As the last optical analysis, the optical conductivity (σ_{opt}) of the samples was determined according to Equation (8).

$$\sigma_{opt} = \alpha nc/4\pi \tag{8}$$

where c is the speed of light in a vacuum. As is known, optical conductivity describes how well a material can conduct electric current in response to the absorption of electromagnetic radiation, particularly in the optical frequency range. The variations of optical conductivity with wavelength in the UV–Vis range have also been given for the samples in Figure 11.

As is known, when a material absorbs light with energy equal to or greater than its band gap, the material can raise electrons from the valence band to the conduction band, creating electron–hole pairs. Optical conductivity is a measure of the ability of these electron–hole pairs to conduct electric current. From this perspective, according to Figure 11, the Bi_2O_3 nanoparticle contribution gradually increases the optical conductivity of the PP matrix. For example, the optical conductivity increased by 7.12, 10.70, and 13.33 times at 400, 600, and 800 nm, respectively, for 5% Bi_2O_3 nanoparticle doping. However, since PP is essentially an electrically insulating material, the optical conductivity could only increase from 10^5 (S^{-1}) to 10^6 (S^{-1}) with the contribution of 5% Bi_2O_3 nanoparticles between 200 and 350 nm.

3.3 | Analyses of the Frequency-Dependent Electrical Properties of the Pure PP and the Composites

In the context of the frequency-dependent electrical properties of the pure PP and the PP-based composites, the real and imaginary parts of complex permittivity and ac conductivity properties were evaluated. The complex electrical permittivity function $\varepsilon^* = \varepsilon' + j\varepsilon''$ where $= \sqrt{-1}$, the ε' and ε'' are the real and imaginary components of the function, respectively.

$$\varepsilon' = Cd\left(\varepsilon_o A\right)^{-1} \tag{9}$$

$$\varepsilon'' = \varepsilon' \tan\delta \tag{10}$$

In Equations (9) and (10), ε_o is the permittivity of free space, C is the capacitance, d is the thickness of the dielectric material, A is the surface area of the electrodes used in impedance measurements, and $\tan\delta$ is the loss tangent. The real part of the complex electrical permittivity function describes the ability to store electrical energy in an electric field of the dielectric material, whereas the imaginary part of the complex electrical

10974628, 0, Downloaded from https://onlinelibrary.wiley.com/doi/10.1002/app.58192 by Zeynep Guven Ozdemir - Yildiz Teknik University , Wiley Online Library on [08/11/2025]. See the Terms and Conditions (https://onlinelibrary.wiley.com/terms-and-conditions) on Wiley Online Library for rules of use; OA articles are governed by the applicable Creative Commons License

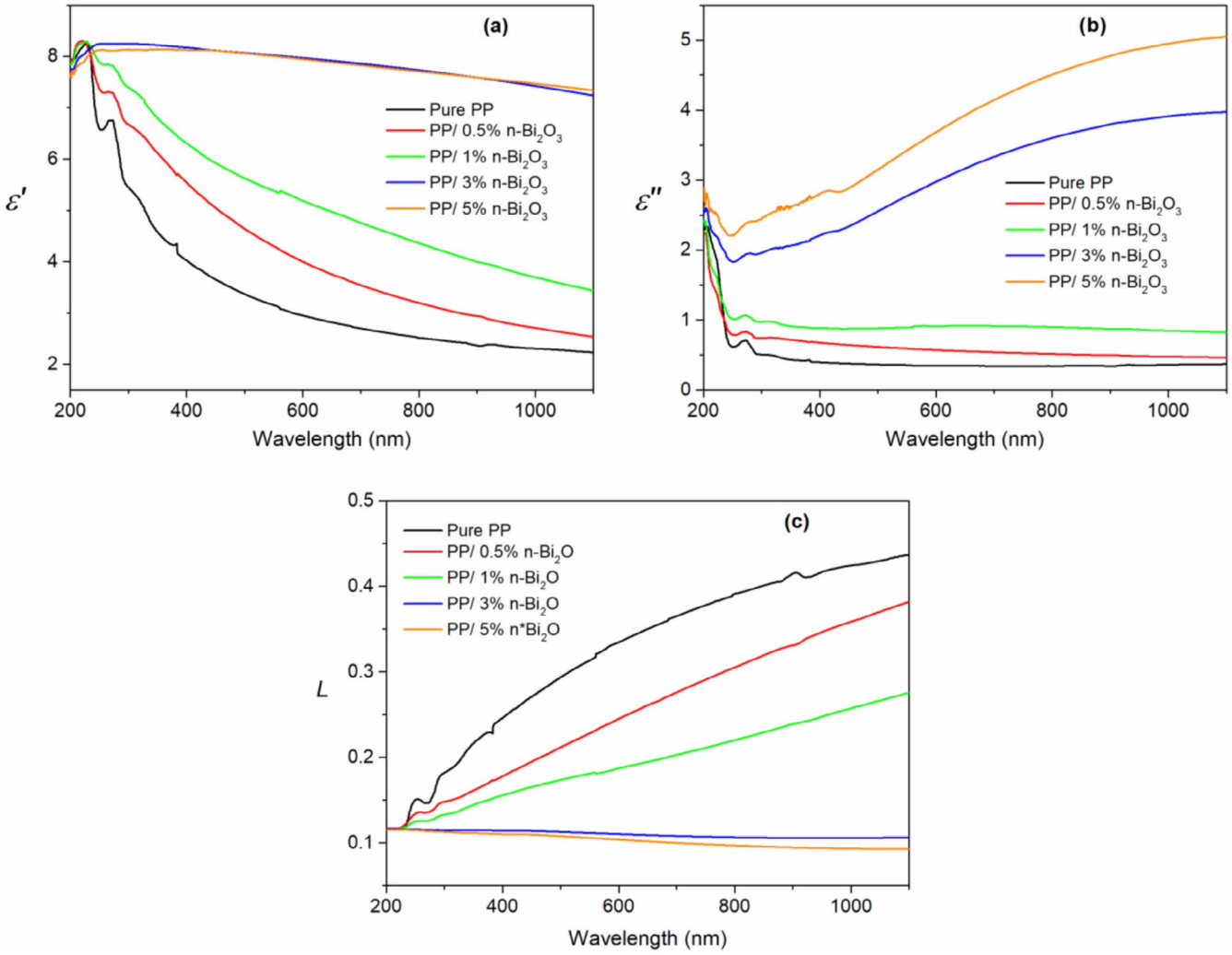


FIGURE 10 | The variations of (a) the real and (b) imaginary parts of the dielectric constant and (c) electron energy loss function of the samples at the UV–Vis wavelength range. [Color figure can be viewed at wileyonlinelibrary.com]

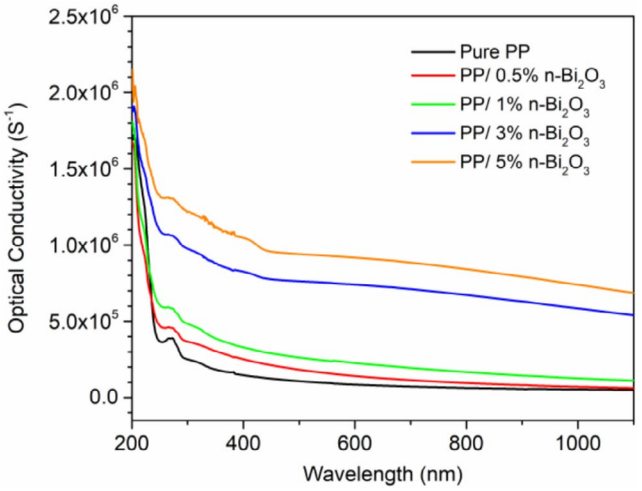


FIGURE 11 | The optical conductivity versus wavelength of the samples in the UV–Vis range. [Color figure can be viewed at wileyonlinelibrary.com]

permittivity function relates to the part of the energy that the dielectric material absorbs from the applied electric field and converts it into heat. Hence, a general opinion can be obtained in terms of the energy storage capability of a dielectric material as a result of considering both ε' and ε'' parameters together.

In Figure 12a, the frequency dependences of the real part of the complex electrical permittivity function of pure PP and the Bi_2O_3 nanoparticle-reinforced PP composites are shown. As shown in Figure 12a, the real part of the complex electrical permittivity of the pure PP exhibits almost frequency-independent response to increasing frequency between 50 Hz and 0.1 MHz. This behavior of the pure PP and the constant value of ε' determined as 1.77 are consistent with the scientific literature [43, 44]. Additionally, since the Bi_2O_3 nanoparticles were doped to PP in small weight ratios, the characteristic of the ε' versus frequency curve of the pure PP as also been preserved in the composites. On the other hand, an increase in ε' values was observed with increasing Bi_2O_3 nanoparticle contribution. When the experimentally measured $\varepsilon' = 1.77$; $\varepsilon' = 1.93$; $\varepsilon' = 1.95$; $\varepsilon' = 1.96$ values for the pure PP, PP/0.5% n-Bi_2O_3, PP/1% n-Bi_2O_3, and PP/5% n-Bi_2O_3 samples, respectively, are evaluated, there is a hierarchical increase in ε' values depending on the Bi_2O_3 contribution. A higher ε' value than pure PP has also been recorded in the case of 3% Bi_2O_3 nanoparticle addition. Hence, it can be concluded that the nano Bi_2O_3 particle additive to PP

10974628, 0, Downloaded from https://onlinelibrary.wiley.com/doi/10.1002/app.58192 by Zeynep Guven Ozdemir - Yildiz Teknik University , Wiley Online Library on [08/11/2025]. See the Terms and Conditions (https://onlinelibrary.wiley.com/terms-and-conditions) on Wiley Online Library for rules of use; OA articles are governed by the applicable Creative Commons License

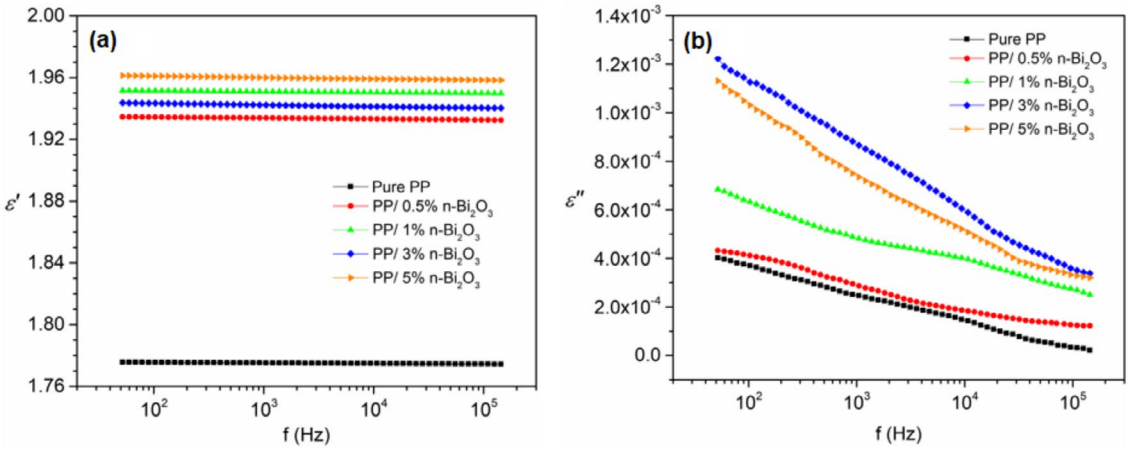


FIGURE 12 | The frequency dependences of the (a) real part and (b) the complex electrical permittivity function of the pure PP and the Bi_2O_3 nanoparticle reinforced PP composites. [Color figure can be viewed at wileyonlinelibrary.com]

leads to higher ε' values, that is, enhanced charge storage ability for the PP matrix. This also confirms the idea that the inclusion of nanoparticles, which is a more conductive additive material than polymer matrix, may result in an increase in the real part of the complex electric permittivity function [45]. As is known, due to their high surface area/volume ratio nanoparticles cause a large interfacial area between the polymer and the nanoparticle in nanopolymer composites. Therefore, since this interaction region is likely to overlap with relatively low-volume fractions in nanocomposites, a small amount of nanoparticle doping leads to significant effects on the electrical behavior of the polymer [46]. On the other hand, it has also been reported in some studies that these interaction regions around the particles allow new charge distributions by forming partially overlapping "semiconductor" regions in nanocomposites [47]. When all these considerations are taken together, it can be thought that the Bi_2O_3 contribution to PP allows for the formation of regions that can be more polarized by the externally applied electric field by allowing new charge distributions, thus causing an increase in ε'.

In Figure 12b, the variation of the imaginary component of the complex electrical permittivity function with frequency was shown for the pure PP and PP/Bi_2O_3 nanocomposites. Experimental data indicate that the pure PP and composites have an extremely low dielectric loss, and the loss increases slightly with increasing Bi_2O_3. This situation is related to enhanced interfacial polarization due to the Bi_2O_3 additive. In this context, the adjective "low-loss" or "nonabsorbing" materials can be used for pure PP and composites, because they are more efficient at storing electrical energy without dissipating it as heat.

As the last electrical parameter, frequency-dependent electrical conductivity was examined. The ac conductivity was calculated by $\sigma_{ac} = \omega\varepsilon_o\varepsilon'' \left(S^{-1}\right)$ where ω is the angular frequency. The variation of conductivity of the pure PP matrix with both frequency and the contribution of Bi_2O_3 was shown in Figure 13.

As is illustrated in Figure 13, all samples including pure PP display strong frequency-dependent electrical conductivity. The strong frequency dependence of the conductivity of polymers can be explained as follows. At low frequencies, the motion of the charge

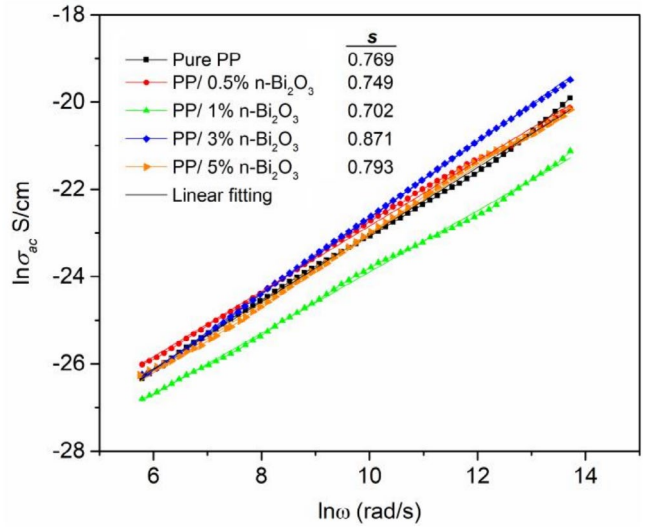


FIGURE 13 | The frequency dependences of the conductivity of the pure PP and the Bi_2O_3 nanoparticle reinforced PP composites. [Color figure can be viewed at wileyonlinelibrary.com]

carriers is hindered by the presence of trapping sites or other barriers in the matrix. However, at higher frequencies, the charge carriers are able to overcome these barriers more easily and move more freely through the material, resulting in an increase in conductivity. Additionally, at higher frequencies, the electric field induces more rapid oscillations of the polymer chains themselves, which can also contribute to an increase in the mobility of the charge carriers and thus an increase in conductivity. On the other hand, the value of the conductivity also shows the poor electrical conductivity of the samples (see Figure 13). The frequency dependences of the conductivity of the samples also suggest Joncher's universal power law (JUPL). JUPL is an empirical relationship that describes the frequency dependence of dielectric relaxation in a wide variety of materials, including solids, liquids, and polymers, and suggests that the frequency dependence of the conductivity is defined as

$$\sigma_{ac} = \sigma_{dc} + A\omega^s \tag{11}$$

where σ_{dc} is the direct current conductivity part, which has not been observed for our samples. In Equation (11), s is the

10974628, 0, Downloaded from https://onlinelibrary.wiley.com/doi/10.1002/app.58192 by Zeynep Guven Ozdemir - Yildiz Teknik University , Wiley Online Library on [08/11/2025]. See the Terms and Conditions (https://onlinelibrary.wiley.com/terms-and-conditions) on Wiley Online Library for rules of use; OA articles are governed by the applicable Creative Commons License

frequency exponent, which usually takes values between 0 and 1. Additionally, A is a constant that depends on the material studied.

As is tabulated in Figure 13, the frequency exponent varies between 0.70 and 0.87. Additionally, the highest conductivity at the mid-and high-frequency range was achieved for the 3% Bi_2O_3 nanoparticle concentration. The increase in conductivity due to the addition of Bi_2O_3 can be explained by providing additional free charge carriers that can move through the PP matrix. Since Bi_2O_3 is a highly polarizable material, meaning that it can induce a large dipole moment in nearby molecules or atoms, this electric dipole moment can create a localized electric field that can ionize molecules in the polymer matrix and generate free charge carriers.

3.4 | Analyses of the Mechanical Properties of the Pure PP and the Composites

Upon the determination of how much the Bi_2O_3 nanoparticle additive improved the mechanical properties of PP, a semicrystalline thermoplastic polymer, mechanical tensile tests were carried out. Samples in thick strips were cut in the dimensions shown in Figure 14 in accordance with ASTM D638-10 (Type 5) standard. The films in the sizes shown in Figure 14 were cut from three different regions of each sample and a mechanical tensile test was performed for each of them. With the help of stress-% strain curves obtained from mechanical tensile tests, Young's modulus, tensile strength, toughness, stress at break, and strain at break values were calculated, and the arithmetic mean of each parameter was determined.

Since PP is a semicrystalline polymer, it contains both crystalline and amorphous regions. Since the molecular chains in the crystalline regions in PP are regular, it is not easy for these chains to wind up or slip. On the other hand, molecular chains in amorphous regions are more entangled. Accordingly, amorphous regions are available to form entangled chains, linked molecules, and other structures. As is known, the denser the entanglement and the greater the number of bonding molecules, the greater the mechanical properties of the material [37]. Since the entanglement of molecular chains requires considerably high energy, it develops the mechanical tensile properties of plastic materials [48]. In addition to this entanglement phenomenon, in semi-crystalline polymers such as PP, the chain morphology of the crystalline region also plays a decisive role in the mechanical properties of the materials. The reflection of these above-mentioned properties of PP on the stress–% strain curves obtained from mechanical tensile tests is as in Figure 14.

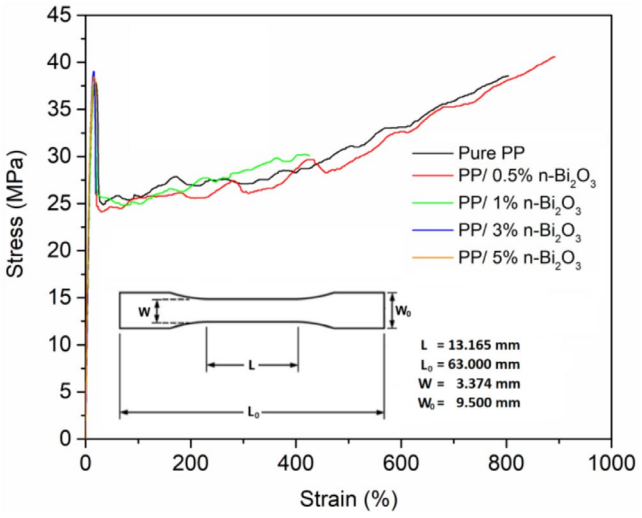


FIGURE 14 | The stress versus % strain curves of the pure PP and the Bi_2O_3 nanoparticle-reinforced PP composites. [Color figure can be viewed at wileyonlinelibrary.com]

As illustrated in Figure 14, the pure PP exhibited the following characteristics: At low levels of stress, PP behaved elastically, meaning that it returned to its original shape when the stress is removed. In this region, the stress–strain curve was a straight line. As stress is increased, the PP material has reached its yield point, accompanied by a sharp drop in stress, where it undergoes plastic deformation. After the yield point, the PP matrix has entered a region of strain hardening, where the stress increases with increasing strain. This is due to the PP polymer chains becoming oriented in the direction of the applied stress, resulting in increased resistance to deformation. At higher levels of applied stress, the cross-sectional area of the PP sample has decreased significantly. Eventually, the PP film reached its ultimate strength, and then it broke. Moreover, the same mechanical response was observed for PP-based nanocomposites, but as given in Table 1, the values of the mechanical parameters changed.

From the data in Table 1, when the development of Young's modulus of PP with the contribution of nanoparticles is considered alone, it was observed that Young's modulus reached its highest value by increasing 49.5% with the contribution of 5% n-Bi_2O_3. Therefore, the PP/5% n-Bi_2O_3 composite with the highest Young's modulus observed will deform 49.5% less when subjected to the same amount of stress compared to the pure PP.

Tensile strength also shows how much tension the material can withstand before it deforms. In this context, the highest tensile strength value was obtained with 3% n-Bi_2O_3 contribution; however, a higher tensile strength than PP was observed with 5% n-Bi_2O_3 addition. In this respect, when Young's modulus and tensile strength development are considered together, the 5% n-Bi_2O_3 contribution has added stiffness and rigidity to PP in terms of mechanical properties and has made positive contributions to its functionality in areas such as packaging, construction, and automotive industries where high strength and durability are important factors.

In the toughness parameter, which indicates how much energy a material can absorb per square meter, it was determined that a high Bi_2O_3 contribution such as 5% has negative effects, but at an extremely low nanoparticle contribution of 0.5%, toughness develops, albeit slightly, compared to pure PP. When stress at break and strain at break are considered together as the final mechanical parameters, the highest values, in other words, the best improvement were recorded at 0.5% Bi_2O_3 nanoparticle contribution, and very sharp decreases were observed in the subsequent contribution percentages, especially strain at break. In this respect, it can be stated that 1% or greater Bi_2O_3 nanoparticle additives make PP weaker and more brittle. These observations are consistent with the

10974628, 0, Downloaded from https://onlinelibrary.wiley.com/doi/10.1002/app.58192 by Zeynep Guven Ozdemir - Yildiz Teknik University , Wiley Online Library on [08/11/2025]. See the Terms and Conditions (https://onlinelibrary.wiley.com/terms-and-conditions) on Wiley Online Library for rules of use; OA articles are governed by the applicable Creative Commons License

TABLE 1 | The mechanical parameters of the pure PP and PP-based nanocomposites.

Samples	Young modulus (MPa)	Tensile strength (MPa)	Toughness (kJm^{-2})	Stress at break (MPa)	Strain at break (%)
Pure PP	323 ± 7.49	37.8 ± 0.88	243 ± 5.64	38.5 ± 0.89	803 ± 18.63
PP/0.5% n-Bi_2O_3	382 ± 12.15	37 ± 1.18	271 ± 8.62	40.5 ± 1.29	892 ± 28.37
PP/1% n-Bi_2O_3	360 ± 9.36	37.3 ± 0.97	118 ± 3.07	30.1 ± 0.78	423 ± 10.99
PP/3% n-Bi_2O_3	397 ± 10.32	39 ± 1.05	6.63 ± 0.17	25 ± 0.65	21 ± 0.55
PP/5% n-Bi_2O_3	483 ± 17.39	38.3 ± 1.38	7 ± 0.25	34.6 ± 1.25	21 ± 0.76

general trend that the incorporation of rigid fillers enhances the stiffness of the host matrix, as also reported for PP hybrids with talc/perlite systems and for metal-matrix hybrids prepared by stir casting [49, 50]. In this context, these polymer composites with enhanced toughness and ductility can be used in packaging applications to protect fragile products during transportation and handling. Additionally, they can be utilized in the automotive and construction industries. In light of all the comments, PP-based nanocomposite reinforced with either 0.5% Bi_2O_3 or 5% Bi_2O_3 can be preferred in accordance with the application in which they will be used.

4 | Conclusions

In this study, it was planned to increase the functionality of PP by strengthening it with Bi_2O_3 nanoparticles (n-Bi_2O_3). For this purpose, the nano-sized Bi_2O_3 was synthesized by the solvothermal method and structurally analyzed by XRD and TEM. Nanocomposites were produced in thick film form by adding nanoparticles to the PP matrix at rates ranging from 0.5% to 5% by mass, using extruder and hot press techniques. The obtained nanocomposites were analyzed chemically by FTIR. In the first part of the study, the UV–Vis light absorption, transmittance, and reflectance spectra of the samples were evaluated. UV–Vis light analysis has shown that the band gap values of the composites were lower than pure PP; on the other hand, it was shown that increasing Bi_2O_3 contribution causes a gradually increasing refractive index and extinction coefficient. Additionally, it was determined that the optical conductivity of PP increased with the addition of Bi_2O_3 nanoparticles. Then, in the second part, the electrical properties of the nanocomposites have also been investigated with an impedance analyzer in the frequency range of 50 Hz–0.1 MHz at room temperature. These electrical properties include real and imaginary components of complex electrical permittivity and ac conductivity. It was shown that the real part of the complex electrical permittivity function can be improved with the Bi_2O_3 nanoparticle doping. Finally, in the third part of the study, the mechanical properties (Young's modulus, tensile strength, toughness, stress at break, and strain at break) of the produced composite set were determined by mechanical tensile tests. The 5% Bi_2O_3 additive percentage also increased Young's modulus of PP at the maximum level, giving it more advanced stiffness and rigidity. In this regard, 5% Bi_2O_3 addition improved both the electrical energy storage properties of PP in the range of 50 Hz–0.1 MHz and increased Young's modulus to the maximum level. Furthermore, it was also observed that if Bi_2O_3 nanoparticle is added to PP as low as 0.5%, it leads to the maximum improvement in stress at break and strain at break. In addition, wettability measurements showed that 0.5 wt% Bi_2O_3 caused a hydrophobic transition, while higher loadings induced a return to hydrophilic behavior. This wetting behavior is consistent with AFM roughness trends and reflects a Cassie–Baxter to Wenzel regime transition, highlighting the tunable surface properties of the composites. In conclusion, PP/Bi_2O_3 nanocomposites synthesized via solvothermal and melt-processing techniques demonstrated simultaneous enhancements in optical, dielectric, and mechanical properties. These multifunctional improvements make the developed nanocomposites promising candidates for advanced dielectric energy storage devices, durable flexible packaging, and lightweight automotive components. The results provide a useful perspective on understanding polymer-nanoparticle systems that address application-specific requirements.

Author Contributions

Emre Beyazay: formal analysis (equal), investigation (equal). **Nazlıcan Şahin Sütcü:** formal analysis (equal), investigation (equal). **Ayşe Nur Şahin:** formal analysis (equal), investigation (equal). **Yaşar Karabul:** investigation (equal), methodology (equal). **Mehmet Kılıç:** conceptualization (equal), software (equal), supervision (equal), validation (equal). **Zeynep Güven Özdemir:** conceptualization (equal), project administration (lead), supervision (equal), writing – original draft (equal), writing – review and editing (equal).

Acknowledgments

This research was supported by Yildiz Technical University Scientific Research Projects Coordination Department with Project Number FBA-2020-4003.

Conflicts of Interest

The authors declare no conflicts of interest.

Data Availability Statement

The data that support the findings of this study are available on request from the corresponding author. The data are not publicly available due to privacy or ethical restrictions.

References

1. C. Y. Chee, N. Song, L. C. Abdullah, T. S. Choong, A. Ibrahim, and T. Chantara, "Characterization of Mechanical Properties: Low-Density Polyethylene Nanocomposite Using Nanoalumina Particle as Filler," *Journal of Nanomaterials* 2012 (2012): 118.

10974628, 0, Downloaded from https://onlinelibrary.wiley.com/doi/10.1002/app.58192 by Zeynep Guven Ozdemir - Yildiz Teknik University , Wiley Online Library on [08/11/2025]. See the Terms and Conditions (https://onlinelibrary.wiley.com/terms-and-conditions) on Wiley Online Library for rules of use; OA articles are governed by the applicable Creative Commons License

2. C. Y. Chee and I. I. Yaacob, "Influence of Nano-SiO_2/Polyamide Composites Coating on Thermic Effect and Optical Properties of Polyethylene Film," *International Journal of Modern Physics B* 23 (2009): 1395–1400.

3. C. Y. Chee and I. I. Yaacob, "Influence of Nanosilica/Polyurethane Composite Coating on IR Effectiveness and Visible Light Transmission Properties of Polyethylene," *Advanced Materials Research* 97 (2010): 1669–1672.

4. Y. C. Ching and I. I. Yaacob, "Effect of Polyurethane/Nano-SiO_2 Composites Coating on Thermo-Mechanical Properties of Polyethylene Film," *Advanced Materials and Processing* 2010 (2011): 161–164.

5. A. Lagashetty and A. Venkataraman, "Polymer Nanocomposites," *Resonance* 10 (2005): 49–57.

6. C. YernChee, Y. C. Ching, and I. Yaacob, "Weathering Resistance of Solventborne Polyurethane/Nanosilica Composite," *Advanced Science Letters* 12 (2012): 165–169.

7. G. Tg, G. Nagaraj, G. Saravanakumar, et al., "Mechanical Performance of ABS/CNT Nanocomposites Developed by Fused Deposition Modelling," *Materials Technology* 40 (2025): 2537746.

8. T. Gangadhar, D. Girish, J. Satheesh, H. Govtham, and K. Pradeep, "Evaluation of Mechanical Properties of Al7029/Flyash/WC Hybrid Composites Developed by Liquid Metallurgy," *Materials Today: Proceedings* 46 (2021): 5969–5974.

9. N. Shivaprasad, M. G. Veena, B. S. Madhukar, et al., "Highly Flexible, Green Luminescent Down Converting and Hydrophobic 0-D Cesium Lead Bromide (Cs_4PbBr_6)/poly (Vinylidene Difluoride) Polymer Nanocomposites for Photonics and Display Applications," *Inorganic Chemistry Communications* 159 (2024): 111761.

10. V. Kumar and A. Singh, "Polypropylene Clay Nanocomposites," *Reviews in Chemical Engineering* 29 (2013): 439–448.

11. M.-J. Khalaj, H. Ahmadi, R. Lesankhosh, and G. Khalaj, "Study of Physical and Mechanical Properties of Polypropylene Nanocomposites for Food Packaging Application: Nano-Clay Modified With Iron Nanoparticles," *Trends in Food Science & Technology* 51 (2016): 41–48.

12. F. Mirjalili, L. Chuah, A. Dayang, M. Hasmaliza, R. Aghababaza, and F. Ahmadun, "Mechanical Properties of α-Al_2O_3/PP Nano Composite," *Journal of Applied Sciences* 9 (2009): 3199–3201.

13. J. Bian, Z. J. Wang, H. L. Lin, X. Zhou, W. Q. Xiao, and X. W. Zhao, "Thermal and Mechanical Properties of Polypropylene Nanocomposites Reinforced With Nano-SiO_2 Functionalized Graphene Oxide," *Composites Part A, Applied Science and Manufacturing* 97 (2017): 120–127.

14. A. Chafidz, M. Kaavessina, S. Al-Zahrani, and M. N. Al-Otaibi, "Rheological and Mechanical Properties of Polypropylene/Calcium Carbonate Nanocomposites Prepared From Masterbatch," *Journal of Thermoplastic Composite Materials* 29 (2016): 593–622.

15. D. Eiras and L. A. Pessan, "Mechanical Properties of Polypropylene/Calcium Carbonate Nanocomposites," *Materials Research* 12 (2009): 517–522.

16. M. Parhizkar, K. Shelesh-Nezhad, and A. Rezaei, "Mechanical and Thermal Properties of Homo-PP/GF/$CaCO_3$ Hybrid Nanocomposites," *Advances in Materials Research* 5 (2016): 121.

17. D. Aydemir, U. Gulsen, H. Gumuş, et al., "Nanocomposites of Polypropylene/Nano Titanium Dioxide: Effect of Loading Rates of Nano Titanium Dioxide," *Materials Science* 22 (2016): 364–369.

18. K. Prashantha, J. Soulestin, M. Lacrampe, et al., "Electrical and Dielectric Properties of Multi-Walled Carbon Nanotube Filled Polypropylene Nanocomposites," *Polymers and Polymer Composites* 18 (2010): 489–494.

19. P. Song, L. Zhao, Z. Cao, and Z. Fang, "Polypropylene Nanocomposites Based on C 60-Decorated Carbon Nanotubes: Thermal Properties, Flammability, and Mechanical Properties," *Journal of Materials Chemistry* 21 (2011): 7782–7788.

20. C.-R. Yu, D.-M. Wu, Y. Liu, et al., "Electrical and Dielectric Properties of Polypropylene Nanocomposites Based on Carbon Nanotubes and Barium Titanate Nanoparticles," *Composites Science and Technology* 71 (2011): 1706–1712.

21. S. Nikmatin, A. Syafiuddin, A. B. Hong Kueh, and A. Maddu, "Physical, Thermal, and Mechanical Properties of Polypropylene Composites Filled With Rattan Nanoparticles," *Journal of Applied Research and Technology* 15 (2017): 386–395.

22. E. Yakkan, T. Uysalman, M. Atagür, K. Sever, and M. Ö. Seydibeyoğlu, "Nanocellulose-Polypropylene Nanocomposites Enhanced With Coupling Agent," *Bartın Orman Fakültesi Dergisi* 20 (2018): 491–502.

23. J. Hu, X. Zhao, J. Xie, Y. Liu, and S. Sun, "Effect of Organic Na+− Montmorillonite on the Dielectric and Energy Storage Properties of Polypropylene Nanocomposites With Polypropylene-Graft-Maleic Anhydride as Compatibilizer," *Journal of Applied Polymer Science* 139 (2022): 52047.

24. A. C. P. Sarturato, E. G. R. Dos Anjos, J. Marini, G. F. D. M. Morgado, M. R. Baldan, and F. R. Passador, "Polypropylene/Talc/Graphene Nanoplates (GNP) Hybrid Composites: Effect of GNP Content on the Thermal, Rheological, Mechanical, and Electrical Properties," *Journal of Applied Polymer Science* 140 (2023): e53657.

25. K. Tserpes, A. Chanteli, S. Pantelakis, E. Koumoulos, and C. Charitidis, "Mechanical and Nanomechanical Properties of MWCNT/PP Nanocomposite," *Frattura Ed Integrità Strutturale* 12 (2018): 73–83.

26. A. Azmi, K. Y. Lau, N. A. Ahmad, et al., "Structure-Dielectric Property Relationship in Polypropylene/Multi-Element Oxide Nanocomposites," *IEEE Transactions on Nanotechnology* 20 (2021): 377–385.

27. B. Lee, U. Hwang, J. Kim, et al., "Highly Dispersed Graphene Nanoplatelets in Polypropylene Composites by Employing High-Shear Stress for Enhanced Dielectric Properties and Frequency-Selective Electromagnetic Interference Shielding Capability," *Composites Communications* 37 (2023): 101409.

28. D. Kanmaz, R. Celen, E. Karaca, and G. Manasoglu, "Investigation of Wettability, Thermal Stability, and Solar Behavior of Composite Films Based on Thermoplastic Polyurethane and Barium Titanate Nanoparticles," *Polymers* 16 (2024): 3259.

29. S. Parvate, P. Dixit, and S. Chattopadhyay, "Superhydrophobic Surfaces: Insights From Theory and Experiment," *Journal of Physical Chemistry B* 124 (2020): 1323–1360.

30. D. Quéré, "Wetting and Roughness," *Annual Review of Materials Research* 38 (2008): 71–99.

31. A. Cassie and S. Baxter, "Wettability of Porous Surfaces," *Transactions of the Faraday Society* 40 (1944): 546–551.

32. Y.-J. Sheng, S. Jiang, and H.-K. Tsao, "Effects of Geometrical Characteristics of Surface Roughness on Droplet Wetting," *Journal of Chemical Physics* 127 (2007): 234704.

33. R. N. Wenzel, "Resistance of Solid Surfaces to Wetting by Water," *Industrial and Engineering Chemistry* 28 (1936): 988–994.

34. N. Mathakari, V. Bhoraskar, and S. Dhole, "A Comparative Study on the Effects of co-60 Gamma Radiation on Polypropylene and Polyimide," *Radiation Effects and Defects in Solids* 169 (2014): 779–790.

35. A. Gopanna, R. N. Mandapati, S. P. Thomas, K. Rajan, and M. Chavali, "Fourier Transform Infrared Spectroscopy (FTIR), Raman Spectroscopy and Wide-Angle X-Ray Scattering (WAXS) of Polypropylene (PP)/cyclic Olefin Copolymer (COC) Blends for Qualitative and Quantitative Analysis," *Polymer Bulletin* 76 (2019): 4259–4274.

36. Ü. Alkan, Y. Karabul, A. E. Bulgurcuoğlu, M. Kılıç, Z. G. Özdemir, and O. İçelli, "Polypropylene/Basalt Thick Film Composites: Structural, Mechanical and Dielectric Properties," *E-Polymers* 17 (2017): 417–425.

37. D. Sinha, T. Swu, S. Tripathy, R. Mishra, K. Dwivedi, and D. Fink, "Spectroscopic and Thermal Studies of Gamma Irradiated

10974628, 0, Downloaded from https://onlinelibrary.wiley.com/doi/10.1002/app.58192 by Zeynep Guven Ozdemir - Yildiz Teknik University , Wiley Online Library on [08/11/2025]. See the Terms and Conditions (https://onlinelibrary.wiley.com/terms-and-conditions) on Wiley Online Library for rules of use; OA articles are governed by the applicable Creative Commons License

Polypropylene Polymer," *Radiation Effects and Defects in Solids* 158 (2003): 531–538.

38. M. Ashokkumar and S. Muthukumaran, "Microstructure and Band Gap Tailoring of $Zn_{0.96-x}Cu_{0.04}CoxO$ ($0 \leqslant x \leqslant 0.04$) Nanoparticles Prepared by Co-Precipitation Method," *Journal of Alloys and Compounds* 587 (2014): 606–612.

39. S. D. Khairnar and V. S. Shrivastava, "Photocatalytic Degradation of Chlorpyrifos and Methylene Blue Using α-Bi_2O_3 Nanoparticles Fabricated by Sol–Gel Method," *SN Applied Sciences* 1 (2019): 1–10.

40. M. Anu and S. S. Pillai, "Structure, Thermal, Optical and Dielectric Properties of SnO_2 Nanoparticles-Filled HDPE Polymer," *Solid State Communications* 341 (2022): 114577.

41. M. G. M. Nion, M. H. Kabir, M. A. Mona, et al., "Effect of Al Doping on Morphology and Optical Properties of Spray Pyrolized MgO Thin Films," *Results in Materials* 12 (2021): 100235.

42. M. H. Kabir, M. Rahman, and M. Khan, "Influence of Al Doping on Microstructure, Morphology, Optical and Photoluminescence Properties of Pyrolytic ZnO Thin Films Prepared in an Ambient Atmosphere," *Chinese Journal of Physics* 56 (2018): 2275–2284.

43. S. Erdönmez and Z. Güven Özdemir, "The Mechanical and Dielectric Properties of Polypropylene Reinforced With $BiSr_2CaCu_2O_{6.5}$ Ceramic," *Polymer Bulletin* 77 (2020): 1793–1812.

44. P. Xu, H. Gui, Y. Hu, A. Bahader, and Y. Ding, "Dielectric Properties of Polypropylene-Based Nanocomposites With Ionic Liquid-Functionalized Multiwalled Carbon Nanotubes," *Journal of Electronic Materials* 43 (2014): 2754–2758.

45. Q. Chi, T. Ma, J. Dong, et al., "Enhanced Thermal Conductivity and Dielectric Properties of Iron Oxide/Polyethylene Nanocomposites Induced by a Magnetic Field," *Scientific Reports* 7 (2017): 3072.

46. T. Tanaka, G. Montanari, and R. Mulhaupt, "Polymer Nanocomposites as Dielectrics and Electrical Insulation-Perspectives for Processing Technologies, Material Characterization and Future Applications," *IEEE Transactions on Dielectrics and Electrical Insulation* 11 (2004): 763–784.

47. T. Lewis, "Nanometric Dielectrics," *IEEE Transactions on Dielectrics and Electrical Insulation* 1 (1994): 812–825.

48. L. Qi, L. Wu, R. He, H. Cheng, B. Liu, and X. He, "Synergistic Toughening of Polypropylene With Ultra-High Molecular Weight Polyethylene and Elastomer-Olefin Block Copolymers," *RSC Advances* 9 (2019): 23994–24002.

49. T. Gangadhar, D. Girish, J. Satheesh, and A. P. Chandra, "Study on Mechanical Properties of Al7050 Alloy Hybrid Composites by Stir Casting Method," *Materials Today: Proceedings* 46 (2021): 5980–5985.

50. A. Yeşilyurt and N. Uysal, "Evaluation of Properties of Polypropylene Matrix Composites Reinforced With Perlite, Expanded Perlite, Silanized Expanded Perlite, and Talc Fillers," *Journal of Applied Polymer Science* 142 (2025): e57695.

10974628, 0, Downloaded from https://onlinelibrary.wiley.com/doi/10.1002/app.58192 by Zeynep Guven Ozdemir - Yildiz Teknik University , Wiley Online Library on [08/11/2025]. See the Terms and Conditions (https://onlinelibrary.wiley.com/terms-and-conditions) on Wiley Online Library for rules of use; OA articles are governed by the applicable Creative Commons License